ACS Appl. Mater. Interfaces, 2016, 8 (9), pp 5752–5757

DOI: 10.1021/acsami.5b11438

Probing the Buried Magnetic Interfaces

Wenqing Liu,[1, 2, 3] *Qionghua Zhou,*[4] *Qian Chen,*[4] *Daxin Niu,*[2] *Yan Zhou,*[1, 3] *Yongbing Xu,*[1, 2, *] *Rong Zhang,*[1, *] *Jinlan Wang,*[4, *] *and Gerrit van der Laan*[5]

[1] York-Nanjing Joint Center (YNJC) for Spintronics and Nanoengineering, School of Electronics Science and Engineering, Nanjing University, Nanjing 210093, China

[2] Spintronics and Nanodevice Laboratory, Department of Electronics, University of York, York YO10 5DD, UK

[3] Department of Physics, The University of Hong Kong, Pokfulam, Hong Kong

[4] Department of Physics, Southeast University, Nanjing 211189, China

[5] Magnetic Spectroscopy Group, Diamond Light Source, Didcot OX11 0DE, UK

[*] Authors to whom correspondence should be addressed. Electronic addresses: yongbing.xu@york.ac.uk, rzhang@nju.edu.cn, and jlwang@seu.edu.cn

Abstract: Understanding magnetism in ferromagnetic metal/semiconductor (FM/SC) heterostructures is important to the development of the new generation spin field-effect transistor (SpinFET). Here, we report an element-specific x-ray magnetic circularly dichroism study of the interfacial magnetic moments for two FM/SC model systems, namely Co/GaAs and Ni/GaAs, which was enabled using a specially designed FM_1/FM_2/SC superstructure. We observed a robust room temperature magnetization of the interfacial Co, whilst that of the interfacial Ni was strongly diminished down to 5 K due to hybridization of the Ni $d(e_g)$ and GaAs sp^3 states. The validity of the selected method was confirmed by *first-principles* calculations, showing only small deviations (<0.02 and <0.07 μ_B/atom for Co/GaAs and Ni/GaAs, respectively) compared to the real FM/SC interfaces. Our work proved that the electronic structure and magnetic ground state of the interfacial FM_2 is not altered when the topmost FM_2 is replaced by FM_1 and that this model is applicable generally for probing the buried magnetic interfaces in the advanced spintronic materials..

Keywords: Spintronics, Interface, XMCD, Superstructure, Magnetic dead layer

A large amount of research effort[1-9] in the spintronics community has been stimulated by the proposal of the spin field-effect transistor (FET)[1] – an analogue of the conventional FETs but with novel capabilities for electronic devices. In the pursuit of such goals, the intrinsic materials' properties are important indicators and the artificially synthetized ferromagnetic metal/semiconductor (FM/SC) heterostructures provide valuable models for studying spin-dependent phenomena and could potentially be used as actual components for eventual spintronic devices. Pioneering work on the creation of non-equilibrium spin structures by means of electrical, optical, and resonance methods pave the way for spin injection. In a FM/SC heterostructure, the best opportunity for spin transport could only be achieved in the absence of a magnetic dead layer at the interface. However, studies on various FM/SC heterojunctions revealed the possibility that the magnetic ordering near a region of the surface or the interface of FM/SC can be strongly altered due to interdiffusion, termination, or hybridization; and controversial reports make this issue rather complex.[2, 3, 4, 5, 6, 7, 8, 9]

The atomic-scale interfacial magnetization of the FM/SC is closely linked with two general questions, namely (*i*) how the magnetic ordering changes with reduced dimensionality and (*ii*) how the magnetic ordering changes due to electronic bonding at the interface with the SC substrate. Direct experimental demonstration of the magnetic state of epitaxial FM/SC interface down to the monolayer (ML) scale remains a nontrivial task, even up to this day, partially due to the inaccessibility of the buried layer (referred to as FM_2 hereafter) between the upper layers (referred to as FM_1 hereafter) and the substrate. On the one hand, for samples comprising of several nanometers thick FM, ambiguities are always present if one tries to separate the contributions from the bulk FM_1 and the interfacial FM_2. On the other hand, minute amounts of FM (in the form of atoms and clusters) will be paramagnetic or ferromagnetic with an extremely low Curie temperature, T_C,[5, 10] and consequently no longer be representative for a terminated surface of a bulk FM on the SC. Moreover, when the FM atoms are reduced to minute amounts, many conventional detection techniques become invalid, as conditions such as vacuum, sensitivity, cryogenics, etc., must be simultaneously satisfied with high strictness.

To overcome these obstacles, we present in this Letter an x-ray magnetic circular dichroism (XMCD)[11] study on a specially designed FM_1/FM_2/SC structure, allowing a clear-cut distinction between the different layers and consequently a direct demonstration of the "real interface". Here, the FM_2 (= Co, Ni) layers are epitaxially deposited on the SC (= GaAs) and then capped with a thick layer of FM_1 (= Fe, Co $\neq FM_2$ in each sample), which serves as the stabilizing layer. The thick FM_1 is chemically distinguishable but magnetically akin to the

FM_2, providing it with a source of exchange interaction. Combined with the unique element selectivity of XMCD, this structure allows direct observation of the interfacial behavior of the bulk FM_2 on the SC [see Fig. 1(a) for illustration]. We initialized this method in the study of Fe/GaAs interface[12] and now we confirm that the electronic structure and magnetic ground state of the interfacial FM_2 would not be altered when the topmost FM_2 is replaced by FM_1 and therefore can be measured directly on the FM_1/FM_2/SC structure.

The 10 ML Cr/7 ML Fe/1 ML Co/GaAs(100) and 10 ML Cr/7 ML Co/1 ML Ni/GaAs(100) samples used in this study were prepared by molecular-beam epitaxy (MBE) using the well-established recipe.[12] The base pressure of the ultra-high vacuum (UHV) chamber is $<1.5\times10^{-10}$ mbar. Prior to the growth, the As-caped GaAs(100) substrate was initially annealed at 340°C to desorb the As capping layer from the surface before further annealing at 550°C for 1 h to promote a clean and ordered Ga-rich surface. Once the system had cooled down to room temperature, Co and Ni were deposited onto the surface at a rate of ~1 ML/min, as monitored by a quartz microbalance calibrated by ex-situ atomic force microscopy (AFM). After the desired thicknesses were achieved, the samples were capped with a different element of several ML, i.e., 7 ML Co atop 1 ML Ni on GaAs and 7 ML Fe atop 1 ML Co on GaAs. Finally, the samples were capped with 10 ML Cr to protect them from oxidation during transport to the synchrotron facility.

X-ray absorption spectroscopy (XAS) and XMCD at the Fe, Co, and Ni $L_{2,3}$ absorption edges were performed on beamline I10 at the Diamond Light Source, UK. XAS was performed in the Faraday geometry, i.e., with the x-rays at normal incidence with respect to the sample surface and parallel to the applied magnetic field, as schematically shown in Fig. 1(b). The XMCD was obtained by taking the difference of the XAS spectra, i.e., $\sigma^- - \sigma^+$, by flipping the x-ray helicity at a fixed magnetic field of 45 kOe, under which the sample is fully magnetized.

Typical pairs of XAS and corresponding XMCD spectra of both samples, normalized to the incident beam intensity, are presented in Fig. 2(a)-(d). The XAS of Fe, Co, and Ni show a white line at each spin-orbit split core level without prominent splitting for both left- and right-circularly polarized x-rays, indicating that the samples have been well protected from oxidation. Strong dichroic XAS were obtained for the 1 ML Co at the Co/GaAs interface, whilst 1 ML Ni at the Ni/GaAs interface shows no appreciable XMCD within experimental accuracy, or in other words, points to a magnetic dead layer. To confirm this, the element-specific XMCD of the 1 ML Ni and the topmost 7 ML Co on the 1 ML Ni/GaAs thin film were measured as a function of the (perpendicular) magnetic field at a temperature down to 5 K. The magnetization of the Co and Ni were monitored using the on- to off-peak ratio at the

L_3 edges and plotted against the field as shown in Fig. 2(e)-(f), respectively. Consistent with the preceding experiment, Ni shows no appreciable magnetic signature, while Co exhibits a clear ferromagnetic hysteresis loop along the hard axis, i.e., the out-of-plane direction.

The element-specific spin (m_{spin}) and orbital (m_{orb}) moments of the two epitaxial thin films were extracted by applying the sum rules[13, 14,15] to the integrated XMCD and summed XAS spectra of the Fe, Co, and Ni $L_{2,3}$ edges. The effective number of valence holes, n_h, was obtained by integrating over the unoccupied density of 3*d*-states, ρ(E), based on the sample configurations and the results are 3.19, 2.29, 2.50, and 1.45 for the stabilizing Fe, interfacial Co, stabilizing Co and interfacial Ni, respectively, in agreement with the previous reports on the Fe, Co, Ni thin films.[12, 14, 15] In order to exclude the non-magnetic part of the XAS spectra an arctangent based step function was used to fit the threshold.[16, 17, 18, 19] As can be seen from Fig. 2(e)-(f), the integration (dashed line) of both XMCD and summed XAS spectra becomes flat within the measured range, providing a proper background offset. The sum-rule derived values for m_{spin} are collected in Table I, from which a significant contrast can be seen between the Co/GaAs and Ni/GaAs interfaces with identical thicknesses. Whilst the 1 ML Co at the Co/GaAs interface shows substantial magnetization, i.e., m_{spin} = (0.97±0.10) μ_B/atom and m_{orb} = (0.17±0.05) μ_B/atom, the 1 ML Ni at the Ni/GaAs interface shows nearly vanishing magnetic moments of m_{spin} = (0.09±0.10) and m_{orb} = (0.07±0.05) μ_B/atom. Apart from the suppressed magnetization of the interfacial FM_2 atoms directly in conjunction with the SC, no strong modification occurs for the topmost FM_1 stabilizing layer. The observed magnetic moments for the 7 ML Fe atop Co, i.e. m_{spin} = (1.93±0.10) and m_{orb} = (0.23±0.05) μ_B/atom are reasonably close to those reported by Xu *et al.*,[20] who obtained m_{spin} = (2.03±0.14) and m_{orb} = (0.26±0.03) μ_B/atom for Fe on GaAs(100). There is also agreement for the 7 ML Co atop Ni with m_{spin} = (1.64±0.10) and m_{orb} = (0.19±0.05) μ_B/atom, which is consistent with m_{spin} = 1.550 and m_{orb} = 0.153 μ_B/atom as reported by Chen *et al.*[15]

Three factors can predominately be responsible for the strongly suppressed m_{spin} observed at the Ni/GaAs interface. The first one is the reduced thickness. As is well known FM materials follow the so-called island growth geometry at low coverage. In other words, Ni atoms at these thicknesses, typically less than a few ML, might be too diffused to interact with each other, even with the backing of the topmost stabilizing layer. Indeed our calculation (described below) confirms that the intermixed interfaces, for which the bcc FM is partially continued into the SC are found to be more stable than the abrupt interfaces. The second factor arises from the stacking of the Ni when epitaxially deposited on GaAs. Among the pioneering investigations, Tian *et al.*[21] performed a series of magneto-optical Kerr effect measurements of Ni/GaAs, which suggested para-ferromagnetism transition occurs at ~1.2 nm for the Ni. Scheck *et al.*[22] used the electrodeposition technique with the intention to

overcome the intermixing at the interface and in this case the Ni film forms a face-centered-cubic (fcc), instead of a body-centered-cubic (bcc) stacking. The third factor is associated with the detrimental interdiffusion between FM and SC atoms. Characterized by x-ray photoelectron spectroscopy, the presence of the As peak in the 6-nm Ni film reveals the occurrence of As diffusion into the Ni layer destroying the magnetic properties of the fcc Ni film and leading to a 20% reduction of the magnetization compared to the bulk value.[22] In the study of the evolution of interface properties of the electrodeposited Ni film upon annealing, a significant increase of As out-diffusion has been observed for annealing temperatures up to 623 K accompanying a rise in the Schottky barrier height, which has been attributed to the Ni-Ga-As compound formation.[23]

The three factors discussed above, namely (*i*) growth geometry, (*ii*) FM atom stacking, and (*iii*) detrimental interdiffusion have rather limited impact on Co/GaAs interface according to our observation. Using high-resolution transmission electron microscopy, Gu *et al.*[24] demonstrated hexagonal-close-packed (hcp)-structured epi-Co on GaAs and Mangan *et al*.[25] observed the coexistence of bcc and hcp phases. Idzerda *et al*.[26] confirmed the bcc structure of Co on GaAs(110) using extended x-ray absorption fine structure[27] and theory suggests that bcc Co is not a metastable phase but a forced structure originating from imperfections.[28] Calculations suggest bulk bcc Co can have an m_{spin} as large as 1.7 μ_B/atom.[29] By careful analyses of the reflection high-energy electron diffraction patterns, Monchesky *et al.*[30] demonstrated a ferromagnetic dead layer associated with the formation of interfacial Co_2GaAs for Co thicknesses <3.4 ML and an abrupt in-plane spin-reorientation transition reorients the magnetization along the [001] direction at 7 ML. It should be noted that the thickness boundaries discussed above should be treated in a quantitative manner, as they are subject to specific growth conditions and substrate configurations. For example, passivating layers, such as S and Sb, have been used to reduce the chemical interaction at the Co/GaAs interface and the latter gives a factor of 2.3 enhancement of the magnetic moment compared to the film deposited on the bare GaAs substrate.[26] In addition, the observed enhancement of m_{orb} can be attributed to the symmetry breaking for the ultrathin films, leading to a lifting of the orbital degeneracy, as previously reported in Fe/GaAs[12] and Fe/InAs.[20]

We proceed to assess the feasibility of the selected FM_1/FM_2/SC geometry to this end. *First-principles* calculations were performed within the framework of density functional theory (DFT) implemented in the Vienna *ab-initio* Simulation Package (VASP). Exchange-correlation interactions were treated within the generalized gradient approximation of the Perdew-Burke-Ernzerhof type. A Monkhorst-Pack mesh of 8×8×4 *k*-points was used to model the Brillouin zone for the electronic structure calculations. All atomic positions are fully relaxed with the conjugate gradient procedure until the residual forces vanished within 0.01

eV/Å. Figure 3(a)-(d) presents the calculated FM/SC superstructures with their three-dimensional interfacial charge-transfer map at the right column. Each unit cell consists of 8 ML FM on 9 ML Ga-terminated GaAs to reconcile the experimental configurations. A vacuum space of 15 Å was set to separate the interactions between neighboring slabs of the unit cells in the [100] direction. Consistent with prior works,[24, 25, 26, 27, 28, 29] we found that bcc Co or Ni are energetically favorable when epitaxially grown on zincblende GaAs(100), due to the perfect in-plane lattice match. Furthermore, the intermixed interfaces, for which the bcc FM is partially continued into the SC are found to be more stable than the abrupt interfaces for both Ni/GaAs and Co/GaAs (see supplementary materials) and hereafter we will only discuss the intermixed configurations. Using the Bader charge analysis, it was observed that in Ni/GaAs on average 0.180 e/(unit cell) is transferred from GaAs to Ni, while in Co/GaAs this is only 0.066 e/(unit cell) due to the different electronegativity of Ni and Co. The electron accumulation quickly decays from the third FM layer onwards (see supplementary materials), which explains why the hybridization has a negligible effect on the topmost FM_1 atoms. Altering the topmost FM_1 with FM_2 does not result in significant changes for the charge transfer (δ), i.e., deviations ~10% per unit cell for both Co/GaAs and Ni/GaAs, as detailed in Table I.

The m_{spin} of 7 ML Fe/ 1 ML Co [Fig. 3(a)] in comparison with 8 ML Co [Fig. 3(b)] and 7 ML Co/1 ML Ni [Fig. 3(c)] and 8 ML Ni [Fig. 3(d)] atop GaAs(100) were calculated and are presented in Fig. 3(e)-(f), respectively. It can be seen that the calculated m_{spin} of the interfacial Co underneath either 7 ML Fe or 7 ML Co is almost identical (variation < 0.02 μ_B/atom). The same applies to the Ni/GaAs interfaces with the calculated m_{spin} variation < 0.07 μ_B/atom for the interfacial Ni. This confirms that the used FM_1/FM_2/SC structure well resembles the interfacial magnetic states of the FM_2/SC, so that the results can be treated in a quantitative manner with high accuracy. Table I compares the XMCD-derived and DFT-calculated m_{spin} of the Ni/GaAs and Co/GaAs interfaces. In agreement with the experiments, the calculations give a robust magnetization of the interfacial Co on GaAs(100) with m_{spin} = 1.56 and 1.65 μ_B/atom for the Co atoms sinking into and floating above the Ga atoms, respectively. In contrast, the magnetization of the interfacial Ni on GaAs(100) is largely lost and only builds up again away from the substrate: The sinking and floating Ni atoms have m_{spin} = 0.11 and 0.20 μ_B/atom, respectively, while the m_{spin} rapidly restores to 0.50 μ_B/atom for the third Ni layer and all the way up to 0.76 μ_B/atom for the eighth Ni layer.

The calculated partial density-of-states (DOS) for the abovementioned four FM/SC superstructures are presented in Fig. 3(g)-(j). As is well known, in the bcc crystal field the 3*d* states of both Co and Ni split into e_g and t_{2g} orbitals. The two higher energy e_g orbitals are not fully filled, and primarily responsible for the net spin polarization or magnetism of these

systems. As can been seen in Fig. 3(g)-(h), the exchange splitting, E_{ex} was taken as the difference of the central value of the calculated DOSs for spin-up and spin-down $d(e_g)$ electrons, respectively. The E_{ex} of the interfacial Co persists up to 1.82 eV upon hybridization with GaAs, whilst that of interfacial Ni rapidly reduces to 0.24 eV. The detailed band structures (see supplementary materials) reveal a strong delocalization of the $d(e_g)$ electrons of the interfacial Ni, which increases the overlap between the Ni *d* and GaAs sp^3 states near the Fermi level (E_F). This overlap strongly cancels the m_{spin} by filling the e_g orbitals, leading to the observed vanishing magnetization of the Ni, whereas it only weakly affects the Co on GaAs. The calculations reveal two important facts: (*i*) the electronic structures and magnetic ground states of the interfacial FM_2 are not altered when the topmost FM_2 is replaced by FM_1 and (*ii*) the hybridization of the FM_2 with the SC atoms can strikingly vary for different FM elements (such as Co and Ni), even when they have similar stacking and intermixing with the SC substrate. The model FM_1/FM_2/SC geometry is applicable for probing both magnetically active and dead layers.

To summarize, we have demonstrated the interfacial magnetic ground state of two model FM/SC systems, i.e., Co/GaAs and Ni/GaAs, and validated the method of using the FM_1/FM_2/SC geometry to retrieve the interface of a bulk FM_2/SC. We oserved a well-retained m_{spin} for epitaxial Co but a vanishing m_{spin} for Ni on GaAs(100), which is attributed to the different hybridization states of the Ni $d(e_g)$ with the GaAs sp^3 states. The observed strong interfacial magnetization of Co is robust even when intermixed with GaAs. Precise DFT calculations have proved the feasibility of the selected method of probing the buried interfaces, giving only small deviations when altering the upper layer FM_2 with FM_1, i.e., <0.02 μ_B/atom for Co/GaAs(100) and <0.07 μ_B/atom for Ni/GaAs(100). Our work demonstrates a valuable model for exploring the electronic and magnetic nature of buried interfaces, which can be generalized to a broad variety of hybrid structures. It gives furthermore direct experimental evidence for the robust interfacial magnetization of Co on GaAs, which is important for finding prime materials for the proposed spintronic devices. The method of probing the buried interface as demonstrated here offers further opportunities to to explore the spin and charge transfer of the FM/SC and their dependence on the surface reconstruction based on such FM_1/FM_2/SC geometry, which can be of interest and can have strong implications for both fundamental physics and emerging spintronic technologies, where the electron's spin is manipulated for the operations of the future fast and energy efficient devices.

Author Information

Corresponding Author

E-mail: yongbing.xu@york.ac.uk, rzhang@nju.edu.cn, and* jlwang@seu.edu.cn

Author Contributions

W. Q. Liu and Q. H. Zhou contributed equally to this work. W. Q. Liu wrote the paper. W. Q. Liu and G. van der Laan performed the XMCD experiment. Q. H. Zhou and Q. Cheng did the DFT calculation. D. X. Niu and Y. Zhou contributed discussions. Y. B. Xu, R, Zhang, and J. L. Wang conceptualized the experiment and supervised the work.

Acknowledgement

This work is supported by the State Key Programme for Basic Research of China (Grants No. 2014CB921101), NSFC (Grants No. 61274102, 21173040, 21373045, 11404056, 21525311), NSFC of Jiangsu (Grants No. BK20130016, BK2012322), UK STFC, DARPA Meso program under contract No.N66001-12-1-4034 and N66001-11-1-4105. Diamond Light Source is acknowledged for beamtime on I10. The authors thank the computational resources at the SEU and National Supercomputing Center in Tianjin.

Supporting Information

Supplementary information detailing abrupt interfaces, band structures, and charge transfer accompanies this paper at http://pubs.acs.org/journal/aamick.

Tables

Method	**XMCD**		**DFT**			
Superstructure (FM_1/FM_2)	$m_{spin}^{FM_1}$ **(μ_B/atom)**	$m_{spin}^{FM_2}$ **(μ_B/atom)**	$m_{spin}^{FM_1}$ **(μ_B/atom)**	$m_{spin}^{FM_2}$ **(μ_B/atom)**	δ **(e/unit cell)**	$E_{ex}^{FM_2}$ **(eV)**
7 ML Fe/1 ML Co	1.93±0.10	0.97±0.10	2.48	1.59	0.066	1.82
8 ML Co		1.55 [15]	1.78	1.60	0.075	1.84
7 ML Co/1 ML Ni	1.64±0.10	0.09±0.10	1.78	0.23	0.180	0.24
8 ML Ni		0.54±0.05 [20]	0.59	0.17	0.206	0.17

Table 1 | Comparison of the XMCD-derived and DFT-calculated m_{spin} values.

References

[1] Datta, S.; Das, B. Electronic Analog of the Electro-Optic Modulator. *Appl. Phys. Lett.* **1990**, *56*, 665.

[2] Li, J.; Wang, Z. Y.; Tan, A.; Glans, P. -a.; Arenholz, E.; Hwang, C.; Shi, J.; Qiu, Z. Q. Magnetic Dead Layer at the Interface between a Co Film and the Topological Insulator Bi2Se3. *Phys. Rev. B* **2012**, *86*, 054430.

[3] Nazir, S.; Cheng, J.; Behtash, M.; Luo, J.; Yang, K. Interface Energetics and Charge Carrier Density Amplification by Sn-Doping in $LaAlO_3$ /$SrTiO_3$ Heterostructure. *ACS Appl. Mater. Interfaces* **2015**, 150623112252009.

[4] Yang, C.-K.; Zhao, J.; Lu, J. Magnetism of Transition-Metal/Carbon-Nanotube Hybrid Structures. *Phys. Rev. Lett.* **2003**, *90* (25), 257203.

[5] Eelbo, T.; Waåniowska, M.; Thakur, P.; Gyamfi, M.; Sachs, B.; Wehling, T. O.; Forti, S.; Starke, U.; Tieg, C.; Lichtenstein, A. I.; Wiesendanger, R. Adatoms and Clusters of 3d Transition Metals on Graphene: Electronic and Magnetic Configurations. *Phys. Rev. Lett.* **2013**, *110*, 136804.

[6] Liu, W. Q.; Wang, W. Y.; Wang, J. J.; Wang, F. Q.; Lu, C.; Jin, F.; Zhang, a.; Zhang, Q. M.; Laan, G. Van Der; Xu, Y. B.; Li, Q. X.; Zhang, R. Atomic-Scale Interfacial Magnetism in Fe/Graphene Heterojunction. *Sci. Rep.* **2015**, *5*, 11911.

[7] Fleet, L. R.; Yoshida, K.; Kobayashi, H.; Kaneko, Y.; Matsuzaka, S.; Ohno, Y.; Ohno, H.; Honda, S.; Inoue, J.; Hirohata, A. Correlating the Interface Structure to Spin Injection in Abrupt Fe/GaAs(001) Films. *Phys. Rev. B - Condens. Matter Mater. Phys.* **2013**, *87*, 024401.

[8] Müller, A.; Ruff, A.; Paul, M.; Wetscherek, A.; Berner, G.; Bauer, U.; Praetorius, C.; Fauth, K.; Przybylski, M.; Gorgoi, M.; Claessen, R. Fe3O4 on ZnO: A Spectroscopic Study of Film and Interface Properties. *Thin Solid Films* **2011**, *520*, 368–373.

[9] Liu, T.; Wang, T.; Reid, A. H.; Savoini, M.; Wu, X.; Koene, B.; Granitzka, P.; Graves, C. E.; Higley, D. J.; Chen, Z.; Razinskas, G.; Hantschmann, M.; Scherz, A.; Sto, J.; Tsukamoto, A.; Hecht, B.; Kimel, A. V; Kirilyuk, A.; Rasing, T.; Du, H. A. Nanoscale Con Fi Nement of All-Optical Magnetic Switching in TbFeCo - Competition with Nanoscale Heterogeneity. *Nano Lett.* **2015**, *15*, 6862.

[10] Brar, V. W.; Decker, R.; Solowan, H.-M.; Wang, Y.; Maserati, L.; Chan, K. T.; Lee, H.; Girit, Ç. O.; Zettl, A.; Louie, S. G.; Cohen, M. L.; Crommie, M. F. Gate-Controlled Ionization and Screening of Cobalt Adatoms on a Graphene Surface. *Nat. Phys.* **2010**, *7*, 43–47.

[11] van der Laan, G.; Figueroa, A. I. X-Ray Magnetic Circular Dichroism-A Versatile Tool to Study Magnetism. *Coord. Chem. Rev.* **2014**, *277-278*, 95–129.

[12] Claydon, J. S.; Xu, Y. B.; Tselepi, M.; Bland, J. A. C.; Van Der Laan, G. Direct Observation of a Bulklike Spin Moment at the Fe/GaAs(100)-4 X 6 Interface. *Phys. Rev. Lett.* **2004**, *93*, 037206–1.

[13] Thole, B.; Carra, P.; Sette, F.; Laan, G. van der. X-Ray Circular Dichroism as a Probe of Orbital Magnetization. *Phys. Rev. Lett.* **1992**, *68*, 1943–1946.

[14] Carra, P.; Altarelli, M. X-Ray Circular Dichroism and Local Magnetic Fields. *Phys. Rev. Lett.* **1993**, *70*, 694–697.

[15] Chen, C. T.; Idzerda, Y. U.; Lin, H.-J.; Smith, N. V; Meigs, G.; Chaban, E.; Ho, G. H.; Pellegrin, E.; Sette, F. Experimental Confirmation of the X-Ray Magnetic Circular Dichroism Sum Rules for Iron and Cobalt. *Phys. Rev. Lett.* **1995**, *75*, 152–155.

[16] Liu, W.; He, L.; Xu, Y.; Murata, K.; Onbasli, M. C.; Lang, M.; Maltby, N. J.; Li, S.; Wang, X.; Ross, C. a.; Bencok, P.; van der Laan, G.; Zhang, R.; Wang, K. L. Enhancing Magnetic Ordering in Cr-Doped Bi2Se3 Using High-TC Ferrimagnetic Insulator. *Nano Lett.* **2015**, *15*, 764–769.

[17] Liu, W. Q.; Xu, Y. B.; Wong, P. K. J.; Maltby, N. J.; Li, S. P.; Wang, X. F.; Du, J.; You, B.; Wu, J.; Bencok, P.; Zhang, R. Spin and Orbital Moments of Nanoscale Fe3O4 Epitaxial Thin Film on MgO/GaAs(100). *Appl. Phys. Lett.* **2014**, *104*, 142407.

[18] Liu, W. Q.; Song, M. Y.; Maltby, N. J.; Li, S. P.; Lin, J. G.; Samant, M. G.; Parkin, S. S. P.; Bencok, P.; Steadman, P.; Dobrynin, A.; Xu, Y. B.; Zhang, R. X-Ray Magnetic Circular Dichroism Study of Epitaxial Magnetite Ultrathin Film on MgO (100). *J. Appl. Phys.* **2015**, *117*, 17E121.

[19] Liu, W.; West, D.; He, L.; Xu, Y.; Liu, J.; Wang, K.; Wang, Y. Atomic-Scale Magnetism of Cr-Doped Bi2Se3 Thin Film Topological Insulators. *ACS Nano* **2015**, *9*, 10237–10243.

[20] Xu, Y. B.; Tselepi, M.; Wu, J.; Wang, S.; Bland, J. a. C.; Huttel, Y.; van der Laan, G. Interface Magnetic Properties of Epitaxial Fe-InAs Heterostructures. *IEEE Trans. Magn.* **2002**, *38*, 2652–2654.

[21] Tian, C. S.; Qian, D.; Wu, D.; He, R. H.; Wu, Y. Z.; Tang, W. X.; Yin, L. F.; Shi, Y. S.; Dong, G. S.; Jin, X. F.; Jiang, X. M.; Liu, F. Q.; Qian, H. J.; Sun, K.; Wang, L. M.; Rossi, G.; Qiu, Z. Q.; Shi, J. Body-Centered-Cubic Ni and Its Magnetic Properties. *Phys. Rev. Lett.* **2005**, *94*, 137210.

[22] Guo, G. Y.; Wang, H. H. Gradient-Corrected Density Functional Calculation of Elastic Constants of Fe , Co and Ni in Bcc , Fcc and Hcp Structures. *chinese J. Phys.* **2000**, *38*, 949–961.

[23] Scheck, C.; Evans, P.; Zangari, G.; Schad, R. Sharp Ferromagnet/semiconductor Interfaces by Electrodeposition of Ni Thin Films onto N-GaAs(001) Substrates. *Appl. Phys. Lett.* **2003**, *82*, 2853.

[24] Gu, E.; Gester, M.; Hicken, R. J.; Daboo, C.; Tselepi, M.; Gray, S. J.; Bland, J. A. C.; Brown, L. M.; Thomson, T.; Riedi, P. C. Fourfold Anisotropy and Structural Behavior of Epitaxial Hcp Co/GaAs(001) Thin Films. *Phys. Rev. B* **1995**, *52*, 14704–14708.

[25] Mangan, M. A.; Spanos, G.; Ambrose, T.; Prinz, G. A. Transmission Electron Microscopy Investigation of Co Thin Films on GaAs(001). *Appl. Phys. Lett.* **1999**, *75*, 346.

[26] Idzerda, Y. U.; Elam, W. T.; Jonker, B. T.; Prinz, G. A. Structure Determination of Metastable Cobalt Films. *Phys. Rev. Lett.* **1989**, *62*, 2480–2483.

[27] Subramanian, S.; Liu, X.; Stamps, R. L.; Sooryakumar, R.; Prinz, G. A. Magnetic Anisotropies in Body-Centered-Cubic Cobalt Films. *Phys. Rev. B* **1995**, *52*, 10194–10201.

[28] Izquierdo, M.; Dávila, M. E.; Avila, J.; Ascolani, H.; Teodorescu, C. M.; Martin, M. G.; Franco, N.; Chrost, J.; Arranz, A.; Asensio, M. C. Epitaxy and Magnetic Properties of Surfactant-Mediated Growth of Bcc Cobalt. *Phys. Rev. Lett.* **2005**, *94*, 187601.

[29] Bagayoko, D.; Ziegler, A.; Callaway, J. Band Structure of Bcc Cobalt. *Phys. Rev. B* **1983**, *27*, 7046–7049.

[30] Monchesky, T.; Unguris, J. Magnetic Properties of Co/GaAs(110). *Phys. Rev. B* **2006**, *74*, 241301.

Figures

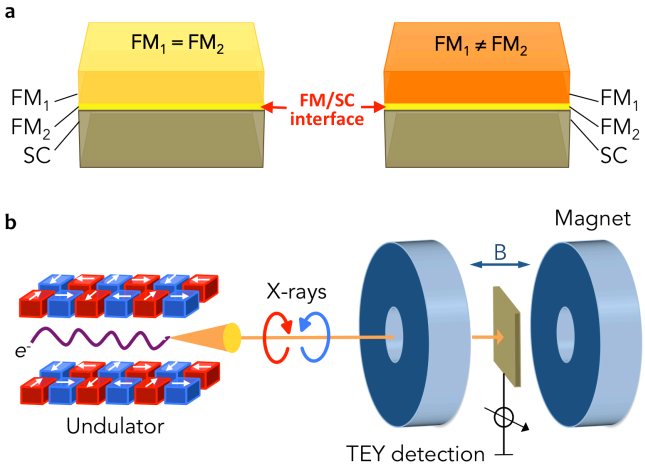

Figure 1. Illustration of the experiment. (a) Illustration of the $FM_1/FM_2/SC$ structure (right) retrieving the FM_2/SC structure (left). (b) Experimental setup for XAS and XMCD, with the beamline optics omitted.

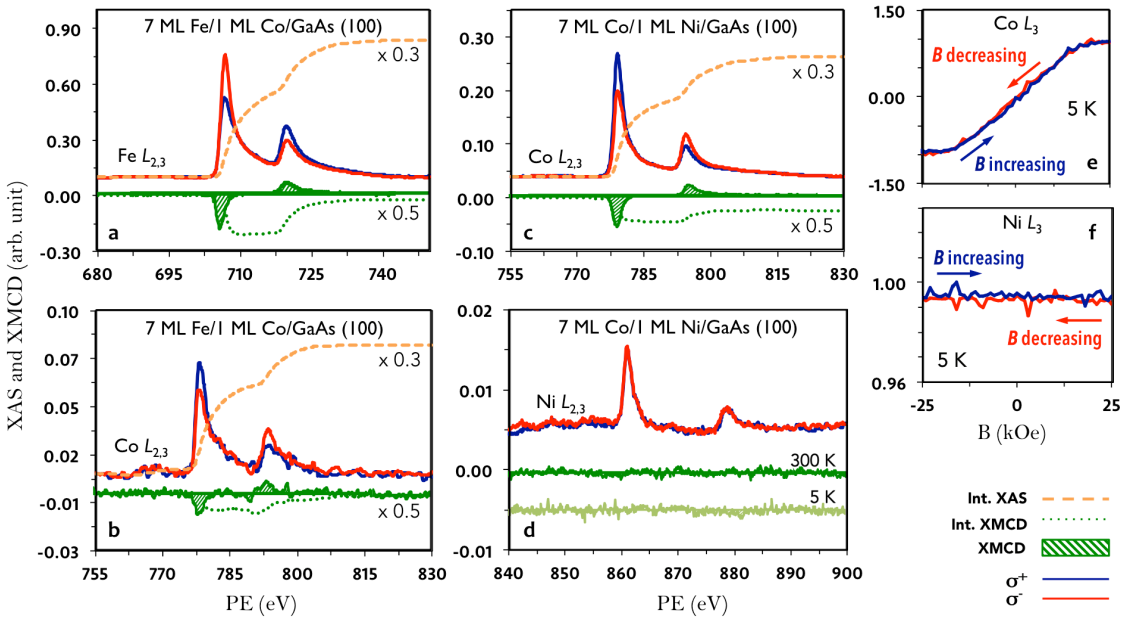

Figure 2. XMCD experimental results. Typical pairs of XAS and XMCD $L_{2,3}$ spectra for (a) Fe and (b) Co of 7 ML Fe/1 ML Co/GaAs(100), and (c) Co and (d) Ni of 7 ML Co/1 ML Ni/GaAs(100). XMCD hysteresis loops of (e) Co and (f) Ni of 7 ML Co/1 ML Ni/GaAs(100) sample at 5 K. Data are offset and scaled for clarity.

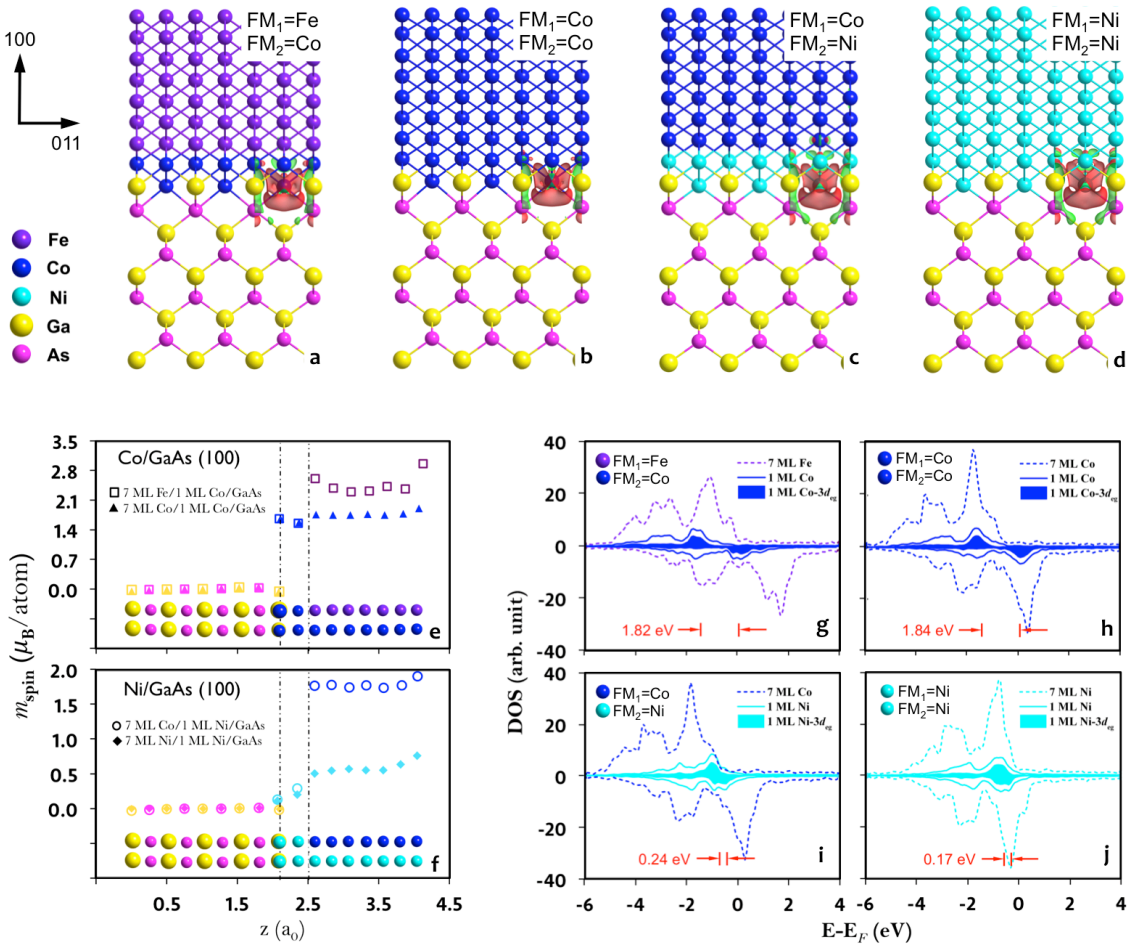

Figure 3. DFT calculational results. (a)-(d) Side view of the FM/SC superstructures, (a) 7 ML Fe/1 ML Co, (b) 8 ML Co, (c) 7 ML Co/ 1 ML Ni, and (d) 8 ML Ni atop GaAs(100) and their 3D differential electronic density map, in which the red and green colored volumes represent charge accumulation and depletion, respectively. The iso-surface corresponds to 0.017 e/Å^3. (e)-(f) Calculated m_{spin} of (e) Co/GaAs and (f) Ni/GaAs interfaces versus distance along the (100) direction. The distance is normalized to the lattice constant of GaAs (a_0 = 5.654 Å). The colored spheres at the bottom indicate the position of each atomic layer. The dashed lines indicate the interfacial or the FM_2 region. (g)-(j) Partial DOS of the four abovementioned FM/SC superstructures and their exchange splitting of the interfacial FM_2.